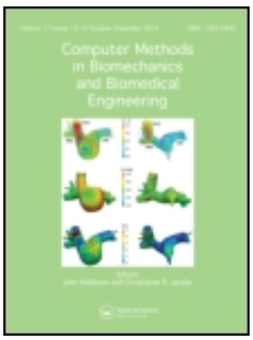

Taylor & Francis
Taylor & Francis Group

Computer Methods in Biomechanics and Biomedical Engineering

ISSN: 1025-5842 (Print) 1476-8259 (Online) Journal homepage: https://www.tandfonline.com/loi/gcmb20

Identification process based on shear wave propagation within a phantom using finite element modelling and magnetic resonance elastography

Gwladys E. Leclerc, Fabrice Charleux, Marie-Christine Ho Ba Tho & Sabine F. Bensamoun

To cite this article: Gwladys E. Leclerc, Fabrice Charleux, Marie-Christine Ho Ba Tho & Sabine F. Bensamoun (2015) Identification process based on shear wave propagation within a phantom using finite element modelling and magnetic resonance elastography, Computer Methods in Biomechanics and Biomedical Engineering, 18:5, 485-491, DOI: 10.1080/10255842.2013.818664

To link to this article: https://doi.org/10.1080/10255842.2013.818664

Published online: 15 Aug 2013.

Computer Methods in Biomechanics and Biomedical Engineering, 2015
Vol. 18, No. 5, 485–491, http://dx.doi.org/10.1080/10255842.2013.818664

Taylor & Francis
Taylor & Francis Group

Identification process based on shear wave propagation within a phantom using finite element modelling and magnetic resonance elastography

Gwladys E. Leclerc[a], Fabrice Charleux[b], Marie-Christine Ho Ba Tho[a] and Sabine F. Bensamoun[a]*

[a]*Laboratoire de BioMécanique et BioIngénierie, Centre de Recherches de Royallieu, Université de Technologie de Compiègne (UTC), UMR CNRS 7338, Rue Personne de Roberval, BP 20529, 60205 Compiègne Cedex, France*
[b]*ACRIM-Polyclinique Saint Côme, Compiègne, France*

(*Received 1 August 2012; final version received 19 June 2013*)

Magnetic resonance elastography (MRE), based on shear wave propagation generated by a specific driver, is a non-invasive exam performed in clinical practice to improve the liver diagnosis. The purpose was to develop a finite element (FE) identification method for the mechanical characterisation of phantom mimicking soft tissues investigated with MRE technique. Thus, a 3D FE phantom model, composed of the realistic MRE liver boundary conditions, was developed to simulate the shear wave propagation with the software ABAQUS. The assumptions of homogeneity and elasticity were applied to the FE phantom model. Different ranges of mesh size, density and Poisson's ratio were tested in order to develop the most representative FE phantom model. The simulated wave displacement was visualised with a dynamic implicit analysis. Subsequently, an identification process was performed with a cost function and an optimisation loop provided the optimal elastic properties of the phantom. The present identification process was validated on a phantom model, and the perspective will be to apply this method on abdominal tissues for the set-up of new clinical MRE protocols that could be applied for the follow-up of the effects of treatments.

Keywords: magnetic resonance elastography; finite element modelling; phantom; identification process; mechanical properties

1. Introduction

Clinical diagnosis established from imaging tests (MRI, CT scan and ultrasound) is primarily based on an analysis of the structural properties of the tissue represented by its texture and morphology (Zuberi et al. 1999; Van Beers et al. 2012). In addition to the common anatomical acquisition, a second image can now reveal the cartography of the tissue stiffness, provided by clinical elastography techniques (Bensamoun et al. 2006, 2008; Shinohara et al. 2010; Niitsu et al. 2011). Thus, the association of the morphological and mechanical properties of the tissue has allowed the clinician to better diagnose, in a non-invasive way, the pathology, such as the stage of fibrosis in the liver (Huwart et al. 2008). To further improve the medical diagnosis, the structural and functional properties were then implemented in constitutive models in order to accurately simulate the tissue behaviour used for surgery training and planning (Mazza et al. 2008; Nava et al. 2008).

Finite element modelling (FEM) was combined with clinical imaging techniques such as elastography, based on the shear wave propagation within the soft tissue, in order to simulate the propagation of the wave. From this displacement, the mechanical properties could be either experimentally measured or numerically determined using finite element (FE) inversion algorithms (Perriez et al. 2010; Doyley 2012). Thus, the V-shaped wave patterns observed in the biceps brachii along the direction of muscle fibres were simulated through 3D-coupled harmonic oscillator calculations (Sack et al. 2002) including the muscle morphology. In addition to the simulation of complex wave patterns, computer models were used to simulate *in vivo* experiments in order to provide an evaluation of the method. Indeed, *in vivo* MRE protocols can be difficult to set-up for certain organs including the brain (Atay et al. 2008; Clayton et al. 2011) or for the analysis of the atherosclerotic plaque (Thomas-Seale et al. 2011).

Since 1995 (Muthupillai et al. 1995), the MRE technique has demonstrated its capability to measure the mechanical properties of a large range of soft tissues (muscle, cartilage, lung, heart and carotid artery) and was recently recognised as a clinical test for the liver. In order to implement other magnetic resonance elastography (MRE) clinical protocols, FEM was used to determine the feasibility of the MRE method to characterise the eye (Litwiller et al. 2010) and the brain (Clayton et al. 2011).

In parallel to *in vivo* experiments performed with MRE, FE simulation was used for the validation of the MRE stiffness measurement (Atay et al. 2008) through the development of different types of gel phantoms (bovine,

*Corresponding author. Email: sabine.bensamoun@utc.fr

agarose and wirosil). Furthermore, phantoms were composed of taut band (Chen et al. 2007) to mimic the wave patterns within the trapezius muscle, or made with inclusions (Glaser et al. 2006) to simulate the tissue behaviour within breast cancer. In addition, various boundary conditions of MRE technique can be tested on a phantom before applying *in vivo* experiments, and the use of FEM aids in understanding the shear wave behaviour (Chen et al. 2005, 2006) leading to the stiffness tissue measurement.

The purpose was to develop an FE identification method for the characterisation of the mechanical properties with MRE technique. This inverse method was validated on a phantom model, mimicking soft tissues, through a simulation of the shear wave propagation performed with an FE model composed of realistic MRE boundary conditions.

2. Materials and methods

2.1 MRE test performed on phantom

It must be noted that the following protocol was described in a previous study (Leclerc et al. 2012) and is briefly summarised here. A homogeneous phantom (diameter = 25 cm, height = 5 cm), composed of 45% softener and 55% liquid plastic (LureCraft, LaGrande, OR, USA) was created to mimic the stiffness of soft biological tissues. The phantom was placed inside a 1.5T MRI machine (GE, Signa HDx, Milwaukee, WI, USA) and shear waves were generated through the phantom with a cylindrical pneumatic driver as shown in Figure 1(A). This driver is composed of a thin flexible membrane (10 μm) made of polycarbonate enclosed by rigid walls (Ehman et al. 2005), and the maximal displacement of the membrane was 39.2 μm for a frequency (f) of 60 Hz (Leclerc et al. 2012). A head coil was used and MRE images were collected with a gradient echo sequence, a flip angle of 45°, a 30 cm × 30 cm field of view and a 256 × 64 acquisition matrix. Four offsets were recorded with a echo time (TE) corresponding to the minimum TE (28 ms) allowing for motion encoding, a repetition time equal to 50 ms and an acquisition time of 38 ms. MRE technique provided phase images showing the shear wave displacement within the phantom (Figure 1(B)). A white profile was manually placed in the radial direction of the shear wave propagation. The wavelength (λ) was measured as the distance between two consecutive peaks, and the elastic property (shear stiffness: μ) of the phantom was calculated with the following equation: $\mu = \rho\lambda^2 f^2$ ($\rho = 1000\,\text{kg/m}^3$ the density of the phantom). It is also assumed that the phantom is composed of an isotropic, homogeneous and elastic media.

2.2 FE models

To simulate the propagation of the shear wave through the phantom, a 3D FE model, composed of two FE models represented by the exciting membrane of the driver (Figure 1(C)) and the phantom (Figure 1(D)), was developed with the software ABAQUS 6.9-1 Standard (Simulia Dassault Systems, Providence, RI, USA).

The FE model of the membrane was represented with the same material properties and boundary conditions as the one that constituted the MRE liver clinical exam (Leclerc et al. 2013). Thus, a cylindrical shell with a 16 cm diameter and a 10 μm thickness (Ehman et al. 2005) was numerically generated (Figure 1(C)). The membrane was meshed with S4R (four-node shell) elements of 10 mm and the prescribed mechanical properties were taken from the literature (Trotignon et al. 1982) and fixed to 2400 MPa for the Young's modulus (E), to 0.37 for the Poisson's ratio (ν) and to 1200 kg/m^3 for the density. Realistic boundary conditions were imposed to the membrane's model, i.e. edges clamped, a mechanical excitation varying sinusoidally at 60 Hz in the Z-direction with a corresponding vertical displacement (U_Z) imposed on each node (Figure 1(C)). This displacement was obtained from the theoretical bending definition for a cylindrical, isotropic, homogeneous plate subjected to a uniform pressure with clamped edges in cylindrical coordinates, associated with a bending rigidity. In a previous study (Leclerc et al. 2012), a mapping of the displacement of the membrane was established and a maximal deflection of 39.2 μm was found at the centre of the membrane, for a mechanical excitation of 60 Hz.

The FE model of the phantom (Figure 1(D)) was modelled as a 3D homogeneous, isotropic cylinder (diameter: 25 cm and height: 5 cm) and different densities, close to the soft tissues, were tested (range: 900–1100 kg/m^3) to match with the experimental shear wave propagation. The FE mesh was composed of C3D8R (eight-node linear brick) elements and different mesh sizes, 10 mm (corresponding to the membrane mesh size), 5 and 2 mm, were tested in order to find a compromise between the accuracy of the simulated displacement and the calculation time. In addition, due to the assumption that the phantom was almost incompressible ($\nu = 0.5$), different Poisson's ratios (0.49, 0.495 and 0.499) were tested. According to the stiffness referenced in the literature (Huwart et al. 2008; Bensamoun et al. 2011) for soft biological tissues, the elastic properties of the phantom, represented by the Young's modulus (E_{Phantom}), varied from 0.1 to 30 kPa ($E = 3\mu$ therefore $0.03 < \mu < 10$ kPa) with an increment of 0.1 kPa.

The FE membrane and the FE phantom models (Figure 1(E)) were combined using a tie constraint in order to observe the propagation of the shear wave through the plastic phantom, and only the outer base of the phantom was fixed in all directions ($U_X = U_Y = U_Z = 0$) (Figure 1(D)). The tie constraint consisted of putting in contact a master surface (membrane) to a slave surface (phantom) in ABAQUS software. To reduce the

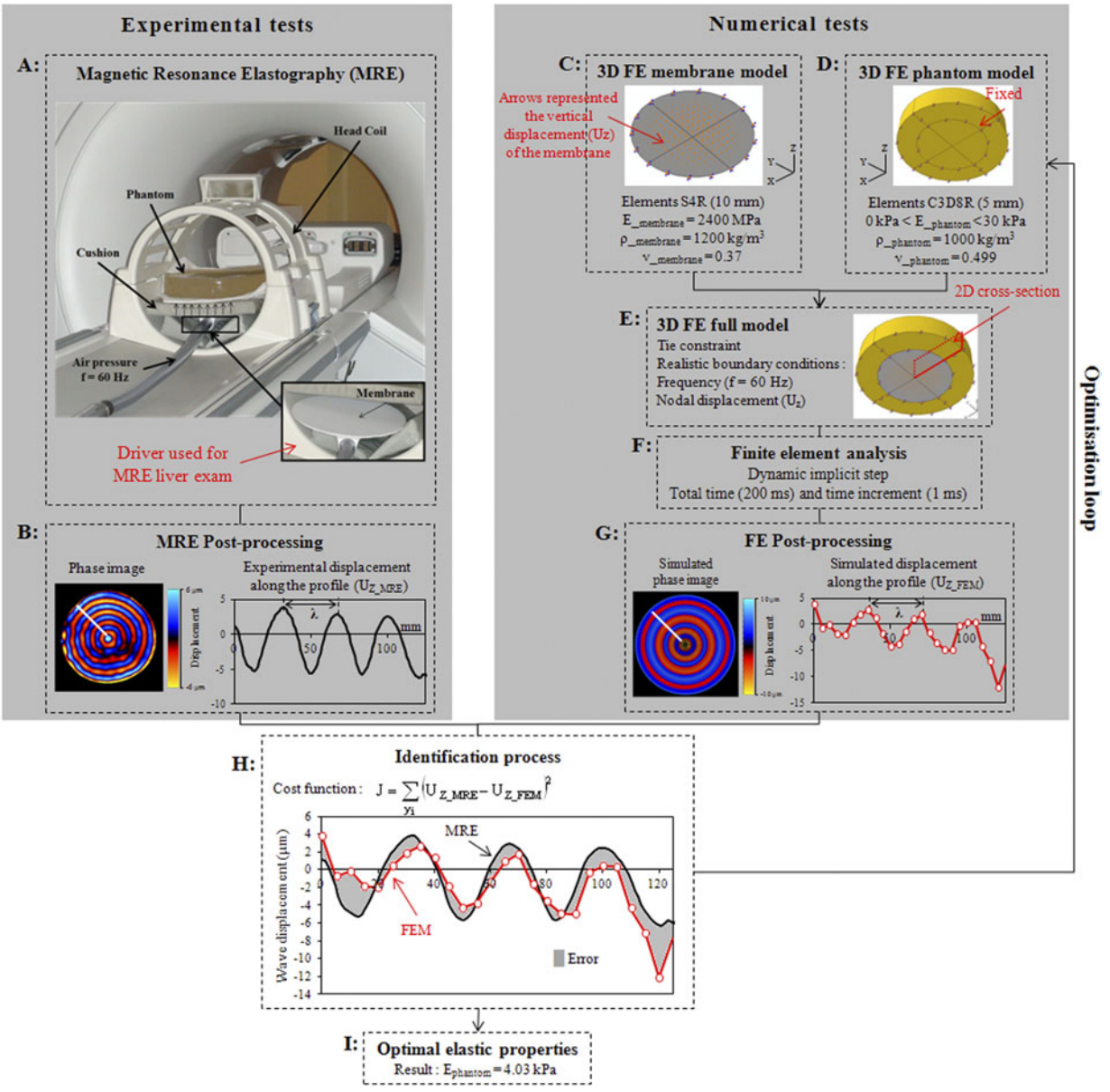

Figure 1. Identification process based on the comparison of the shear wave propagation obtained experimentally, with the MRE technique, and numerically with the development of a finite element model.

resolution time (CPU time) of the 3D FE model, a 2D cross-sectional FE model (Figure 1(E)), represented the membrane and the phantom, was performed with an axisymmetric assumption. The dimensions, the mechanical properties and the boundary conditions of the 2D cross-sectional FE model were the same as those constituted by the 3D FE model, except for the mesh definition of the membrane (nine nodes, eight elements) and the phantom (286 nodes, 250 elements) represented by MAX1 (two-node linear axisymmetric membrane) and CAX4R (four-node bilinear axisymmetric quadrilateral) elements, respectively.

2.3 *FE analysis and identification process*

To visualise the propagation of the shear wave, the FE model was analysed with a dynamic implicit analysis, and the total time was fixed to 200 ms with a time increment of 1 ms (Figure 1(F)). The material damping was assumed to be zero. The simulated propagation of the shear wave was visualised after nine periods in order to obtain a steady state. Similar to the MRE post-processing (Figure 1(B)), a profile was manually placed along the simulated shear wave propagation in order to visualise the simulated wave displacement (U_{Z_FEM}) along the profile (Figure 1(G)).

2.4 Identification process

The identification process (Figure 1(H)) was made with the following cost function (J, mm^2):

$$J = \sum_{y_i} \left(U_{Z\_MRE} - U_{Z\_FEM}\right)^2. \quad (1)$$

A least squared analysis based on the relative error, between the experimental (U_{Z_MRE}) and the 2D numerical (U_{Z_FEM}) wave displacements for each y-abscissa, represented by the grey surface was performed. The discretisation of both splines was constituted with the same number of points.

Then, the optimisation loop was performed and the cost function values were recorded and plotted as a function of the shear stiffness in order to identify the global minimum value revealing the optimal elastic properties of the phantom (Figure 1(I)).

3. Results

3.1 Stiffness measurement with MRE technique

In vitro phase images of the phantom (Figure 1(B)) were obtained with the following boundary conditions: frequency of 60 Hz and displacement of the cylindrical pneumatic driver membrane. The displacement of the shear waves through the phantom was clearly propagated and the measurement of the wavelength revealed a shear stiffness (μ) of 4.16 ± 0.14 kPa corresponding to the material properties of different abdominal tissues such as healthy spleen, healthy kidneys or fibrotic liver.

3.2 Influence of mesh, Poisson's ratio and density on the FE phantom model

The result of the 10 mm mesh size revealed a coarse visualisation of the shear wave displacement along the profile compared to the 5 and 2 mm mesh sizes, which provided optimal simulated displacements. However, the 5 mm was applied due to the increase of the calculation time for elements of 2 mm ($\approx$28000 s) compared to elements of 5 mm ($\approx$918 s). To further reduce the calculation time using the 5 mm elements, the identification process was performed on a 2D FE model leading to a final calculation time of only 9 s.

The comparison between the numerical wave displacements (obtained from the three different Poisson's ratios and densities, Figure 2(A),(B)) and the experimental propagation revealed that the optimal Poisson's ratio and density were 0.499 (Figure 2(A)) and 1000 kg/m^3, (Figure 2(B)), respectively.

3.3 Optimisation of the numerical shear wave displacement

To visualise the simulated propagation of the shear wave within the phantom, the increment time for the FE analysis must be smaller than the period (16.6 ms) corresponding to the mechanical excitation (60 Hz). Thus, the optimal increment was found for 1 ms. In addition, the visualisation of the simulated shear wave propagation was performed at different times (from 150 to 167 ms) in order to identify the optimal time revealing the entire representation of the shear wave behaviour. The results revealed an optimal time of 163 ms corresponding to 9.75 periods.

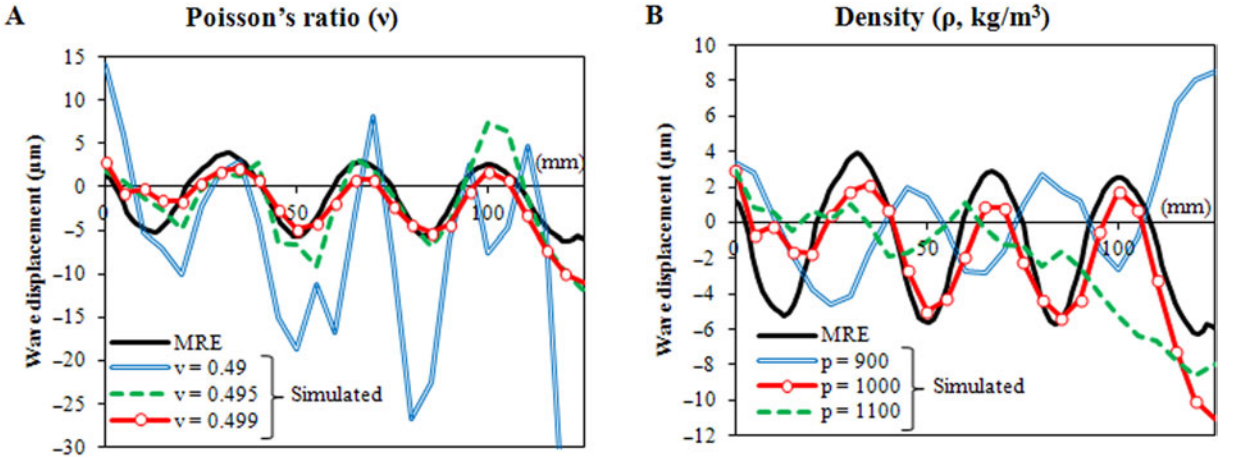

Figure 2. Comparison of the experimental (MRE) and numerical (FE) wave displacements. Different Poisson's ratios (A) and density (B) were tested to find the most representative simulated wave behaviour to the experimental one.

3.4 Comparison of the experimental (MRE) and numerical (FE) shear wave displacements

The results of the identification process revealed a minimum of the cost function ($J = 6.49 \times 10^{-4}$ mm^2) for a Young's modulus of 12.1 kPa, or a shear stiffness of 4.03 kPa (Figure 3). The computational time, to obtain all values of the cost function, was approximately 9000 s. The comparison between the experimental (MRE) and numerical (FE) shear stiffnesses (μ) showed a relative error of 3.1%.

4. Discussion

MRE is a new non-invasive clinical exam prescribed in Europe and the USA (Nguyen and Talwalkar 2011), which improves the diagnosis and treatment of liver disorders and cost-effective prevention. At the beginning of the MRE technique, the elasticity was directly calculated from the phase images with a profile placed locally in the direction of the wave propagation (Rouvière et al. 2006) and subsequently cartography of elasticity were generated from inversion algorithms (Manduca et al. 2001). A recent study has compared the mechanical properties of the liver measured with and without inversion algorithms (Leclerc et al. 2013). It was concluded that the elastic properties calculated from the cartography were underestimated for the severe fibrosis. Therefore, to accurately diagnose a suspicious area, in a case of severe fibrosis, the radiologists may use a profile to locally analyse the tissue. This result showed the complementary of the different MRE post-processing for the purpose of characterising the elastic properties of the liver. Furthermore, a strong variation of the liver viscosity as a function of the MRE post-processing revealed that this parameter should be investigated to demonstrate its relevance in clinical practice (Leclerc et al. 2013).

To further apply this technique for the characterisation of other soft tissues (kidney, spleen and psoas) (Bensamoun et al. 2011), *in vitro* MRE tests were performed on phantoms, allowing the set-up of new MRE protocols and assessing its feasibility. Thus, a phantom was created with a stiffness (about 4 kPa) mimicking different biological tissues such as healthy muscle in a relaxed state (Bensamoun et al. 2006), healthy spleen (Bensamoun et al. 2011) or fibrotic liver (Bensamoun et al. 2013). Therefore, the continuity of this work was to simulate the MRE shear wave propagation within the present developed phantom, using an FE identification method. The originality of this study was to develop an FE model composed, for the first time, of the realistic MRE boundary conditions corresponding to a liver test. Indeed, the sinusoidal displacement induced by the clinical liver driver was quantified with a vibrometer analysis (Leclerc et al. 2012). At that time, MRE studies were currently simulated using unrealistic *in vivo* boundary conditions such as a fixed harmonic displacement (10 μm) applied to the bottom surface of the model (Clayton et al. 2011), an unknown displacement performed at the node located in the middle of the top surface (Chen et al. 2005, 2006), a sinusoidal force made tangent to the top surface (Atay et al. 2008), a uniform displacement of 1.5 mm set on the outer surface nodes (McGrath et al. 2011) or a sinusoidal shear load (2 kN) applied to the nodes (Thomas-Seale et al. 2011).

In addition to the realistic boundary condition, the simulated propagation of the shear wave is also highly influenced by the material properties of the phantom such as density, Poisson's ratio, homogeneity, elasticity and viscosity. Since abdominal tissues are considered to be nearly incompressible and mainly constituted of water, this study took care in testing various values of density and Poisson's ratios in order to develop the closest FE phantom

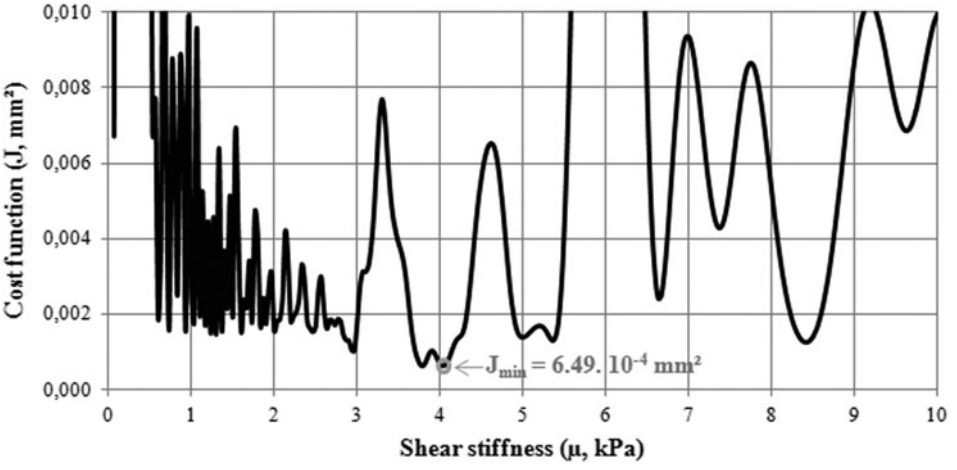

Figure 3. Representation of the cost function (J, mm^2) as a function of the shear stiffness (μ, kPa), which shows the result of the identification process.

model possible for mimicking soft tissues. It must be also noted that the strong assumption of homogeneity was applied in the present FE model as a first step to visualise the shear wave propagation (Chen et al. 2005, 2006). However, this hypothesis should be significantly modified in the future in order to take into account the non-homogeneity properties of the soft biological tissues (Eskandari et al. 2011) and to truly visualise the shear wave propagation. In addition, these tissues were characterised with a viscoelastic behaviour and in this study, the FE model of the phantom was composed of only elastic properties revealing the global elasticity of the tissue using the linear elastic assumption in ABAQUS software. This choice was based on the relevance of this parameter compared to the viscous one that represents the micro-structural changes. Moreover, in the literature (Chen et al. 2005, 2006, 2007; McGrath et al. 2011), most of the MRE FE models were developed only with the elastic properties. In the future, it will be of interest to develop an FE model with the realistic viscoelastic properties of the soft tissues and to analyse the effect of the viscous component on the shear wave propagation. Furthermore, in case of a more complex FE model, the use of a genetic algorithm will be necessary to more rapidly identify the optimal mechanical properties from the minimisation of the cost function.

The present identification process, based on the displacement analysis along a profile, was validated on a phantom model composed of a cylindrical geometry with a homogeneous media and characterised with elastic material properties. To improve this inverse method, these assumptions should be adapted to the biological tissues that are not cylindrical, non-homogeneous and revealed a viscoelastic behaviour. In addition, another perspective will be to adapt this method in order to use the cartography in the identification process. The next step will be to use this validated identification process on different soft tissues. Thus, the simulation of the shear wave propagation will allow the set-up of new clinical MRE protocols that could be applied for the follow-up of the effects of treatments.

Acknowledgement

This work was supported by Region Picardie.

References

Atay SM, Kroenke CD, Sabet A, Bayly PV. 2008. Measurement of the dynamic shear modulus of mouse brain tissue *in vivo* by magnetic resonance elastography. J Biomech Eng. 130:1–11.

Bensamoun SF, Leclerc GE, Debernard L, Cheng X, Robert L, Charleux F, Rhein C, Latrive JP. 2013. Cutoff values for alcoholic liver fibrosis using magnetic resonance elastography technique. Alcohol Clin Exp Res. 37:811–817.

Bensamoun SF, Ringleb SI, Littrell L, Chen Q, Brennan M, Ehman RL, An KN. 2006. Determination of thigh muscle stiffness using magnetic resonance elastography. J Mag Reson Imaging. 23:242–247.

Bensamoun SF, Robert L, Leclerc GE, Debernard L, Charleux F. 2011. Stiffness imaging of the kidney and adjacent abdominal tissues measured simultaneously using magnetic resonance elastography. Clin Imaging. 35:284–287.

Bensamoun SF, Wang L, Robert L, Charleux F, Latrive J-P, Ho Ba Tho M-C. 2008. Measurement of liver stiffness with two imaging techniques: magnetic resonance elastography and ultrasound elastometry. J Magn Reson Imaging. 28: 1287–1292.

Chen Q, Bensamoun SF, Basford JR, Thompson JM, An K-N. 2007. Identification and quantification of myofascial taut bands with magnetic resonance elastography. Arch Phys Med Rehabil. 88:1658–1661.

Chen Q, Ringleb SI, Manduca A, Ehman RL, An K-N. 2005. A finite element model for analyzing shear wave propagation observed in magnetic resonance elastography. J Biomech. 38:2198–2203.

Chen Q, Ringleb SI, Manduca A, Ehman RL, An K-N. 2006. Differential effects of pre-tension on shear wave propagation in elastic media with different boundary conditions as measured by magnetic resonance elastography and finite element modeling. J Biomech. 39:1428–1434.

Clayton EH, Garbow JR, Bayly PV. 2011. Frequency-dependent viscoelastic parameters of mouse brain tissue estimated by MR elastography. Phys Med Biol. 56:2391–2406.

Doyley MM. 2012. Model-based elastography: a survey of approaches to the inverse elasticity problem. Phys Med Biol. 57:R35–R73.

Ehman RL, Rossman PJ, Hulshizer TC, Dresner AM. 2005. Pressure activated driver for magnetic resonance elastography. U.S. Patent 20050270029.

Eskandari H, Salcudean SE, Rohling R, Bell I. 2011. Real-time solution of the finite element inverse problem of viscoelasticity. Inverse Probl. 27(085002):1–16.

Glaser KJ, Felmlee JP, Ehman RL. 2006. Rapid MR elastography using selective excitations. Magn Reson Med. 55:1381–1389.

Huwart L, Sempoux C, Vicaut E, Salameh N, Annet L, Danse E, Peeters F, ter Beek LC, Rahier J, Sinkus R, et al., 2008. Magnetic resonance elastography for the noninvasive staging of liver fibrosis. Gastroenterology. 135:32–40.

Leclerc GE, Charleux F, Robert L, Ho Ba Tho MC, Rhein C, Latrive JP, Bensamoun SF. Forthcoming 2013. Analysis of the liver viscosity behavior as a function of the multi-frequency magnetic resonance elastography (MMRE) post-processing. J Magn Reson Imaging. doi:10.1002/jmri.23986.

Leclerc GE, Debernard L, Foucart F, Robert L, Pelletier KM, Charleux F, Ehman R, Ho Ba Tho M-C, Bensamoun SF. 2012. Characterization of a hyper-viscoelastic phantom mimicking biological soft tissue using an abdominal pneumatic driver with magnetic resonance elastography (MRE). J Biomech. 45:952–957.

Litwiller DV, Lee SJ, Kolipaka A, Mariappan YK, Glaser KJ, Pulido JS, Ehman RL. 2010. MR elastography of the *ex vivo* bovine globe. J Magn Reson Imaging. 32:44–51.

Manduca A, Oliphant TE, Dresner MA, Mahowald JL, Kruse SA, Amromin E, Felmlee JP, Greenleaf JF, Ehman RL. 2001. Magnetic resonance elastography: noninvasive mapping of tissue elasticity. Med Image Anal. 5:237–254.

Mazza E, Grau P, Hollenstein M, Bajka M. 2008. Constitutive modeling of human liver based on *in vivo* measurements. Med Image Comput Comput-Assist Interv. 11:726–733.

McGrath DM, Foltz WD, Al-Mayah A, Niu CJ, Brock KK. 2011. Quasi-static magnetic resonance elastography at 7 T to measure the effect of pathology before and after fixation on tissue biomechanical properties. Magn Reson Med. doi:10.1002/mrm.23223.

Muthupillai R, Lomas DJ, Rossman PJ, Greenleaf JF, Manduca A, Ehman RL. 1995. Magnetic resonance elastography by direct visualization of propagating acoustic strain waves. Science. 269:1854–1857.

Nava A, Mazza E, Furrer M, Villiger P, Reinhart WH. 2008. *In vivo* mechanical characterization of human liver. Med Image Anal. 12:203–216.

Nguyen D, Talwalkar JA. 2011. Noninvasive assessment of liver fibrosis. Hepatology. 53:2107–2110.

Niitsu M, Michizaki A, Endo A, Takei H, Yanagisawa O. 2011. Muscle hardness measurement by using ultrasound elastography: a feasibility study. Acta Radiol. 52:99–105.

Perriez PR, Kennedy FE, Van Houten EEW, Weaver JB, Paulsen KD. 2010. Magnetic resonance poroelastography: an algorithm for estimating the mechanical properties of fluid-saturated soft tissues. IEEE Trans Med Imaging. 29:746–755.

Rouvière O, Yin M, Dresner MA, Rossman PJ, Burgart LJ, Fidler JL, Ehman RL. 2006. MR elastography of the liver: preliminary results. Radiology. 240:440–448.

Sack I, Bernarding J, Braun J. 2002. Analysis of wave patterns in MR elastography of skeletal muscle using coupled harmonic oscillator simulations. Magn Reson Imaging. 20:95–104.

Shinohara M, Sabra K, Gennisson J, Fink M, Tanter M. 2010. Real time visualization of muscle stiffness distribution with ultrasound shear wave imaging during muscle contraction. Muscle Nerve. 42:438–441.

Thomas-Seale LEJ, Klatt D, Pankaj P, Roberts N, Sack I, Hoskins PR. 2011. A simulation of the magnetic resonance elastography steady state wave response through idealised atherosclerotic plaques. IAENG Int J Comput Sci. 38:2636–2639.

Trotignon J-P, Piperaud J, Verdu J, Dobraczynski A. 1982. Precis de matières plastiques: structures, propriétés, mise en oeuvre et normalisation. AFNOR, Nathan, Courbevoie; Paris.

Van Beers B, Doblas S, Sinkus R. 2012. New acquisition techniques: fields of application. Abdom Imaging. 37: 155–163.

Zuberi S, Matta N, Nawaz S, Stephenson J, McWilliam R, Hollman A. 1999. Muscle ultrasound in the assessment of suspected neuromuscular disease in childhood. Neuromuscul Disord. 9:203–207.